Tungsten Hexanitride with Single-Bonded Armchairlike Hexazine Structure at High Pressure

Nilesh P. Salke,[1,*,¶] Kang Xia,[2,3] Suyu Fu,[4] Youjun Zhang,[5] Eran Greenberg,[6] Vitali B. Prakapenka,[6] Jin Liu,[1,†] Jian Sun,[2,‡] and Jung-Fu Lin[4,§]

[1]*Center for High Pressure Science and Technology Advanced Research, Beijing 100094, China*
[2]*National Laboratory of Solid State Microstructures, School of Physics and Collaborative Innovation Center of Advanced Microstructures, Nanjing University, Nanjing 210093, China*
[3]*Department of Applied Physics, College of Science, Nanjing Forestry University, Nanjing 210037, China*
[4]*Department of Geological Sciences, Jackson School of Geosciences, The University of Texas at Austin, Austin, Texas 78712, USA*
[5]*Institute of Atomic and Molecular Physics, Sichuan University, Chengdu 610065, China*
[6]*Center for Advanced Radiation Sources, University of Chicago, Chicago, Illinois 60637, USA*

(Received 30 August 2020; revised 5 December 2020; accepted 22 December 2020; published 8 February 2021)

WN_6 phase discovered at 126–165 GPa after heating of W in nitrogen. XRD refinements reveal a unit cell in space group $R\bar{3}m$ which is consistent with the WN_6 structure with armchairlike hexazine (N_6) rings, while strong A_{1g} Raman mode confirms its N—N single bonds. Density functional theory (DFT) calculations reveal balanced contributions of attractive interactions between W and covalent N_6 rings, and repulsions between N_6 rings that make WN_6 ultrastiff and tough. The WN_6 phase displays long bond lengths in the nearest N-N and pressure-enhanced electronic band gap, which pave the way for finding novel nitrides.

DOI: 10.1103/PhysRevLett.126.065702

Diatomic nitrogen is the most abundant molecule of Earth's atmosphere accounting for almost 78% by volume. The strong triple bond in nitrogen (N ≡ N) makes it highly stable and unreactive at near ambient conditions. At high pressure-temperature (*P-T*) conditions, nitrogen can form double- or even single-bonded solids (N═N, N—N) [1]. Of particular interest is to find single-bonded nitrogen with a huge difference in the average bond energy: the transformation of a single-bonded polymeric nitrogen into a triple-bonded nitrogen molecule is expected to accompany a tremendous energy release [2]. Thus far, searching for single-bonded nitrogen has gained tremendous research interest because of its unique physical properties and potentials in high-energy-density (HED) materials. Previous theoretical predictions and experiments have showed that a number of single-bonded nitrogen allotropes can exist at ultrahigh *P* or *P-T* conditions [1,3–9]. Key observations in past studies include the cubic gauche nitrogen (cg-N) synthesized at ∼110 GPa and ∼2000 K in a diamond anvil cell (DAC) [7], and the hexagonal layered polymeric nitrogen (HLP-N) with tetragonal $P4_2bc$ structure at ∼250 GPa after laser heating [1]. Very recently, black phosphorus structured nitrogen (bp-N) has also been found at 140 GPa after laser heating [3,4]. Particularly, the HLP-N consists of distorted and interconnected hexagonal N_6 rings with N—N single bonds in its structure. Its discovery has renewed the interest of finding the sought-after yet hypothetical planar hexazine N_6 ring of nitrogen, which is argued to be thermodynamically unstable due to the strong lone pair repulsion [10,11].

Nitrogen-bearing compounds have been suggested as a promising means to search for the polymeric N_6 ring at high *P-T* [12–16]. Recently, transition metal nitrides (TMNs) have drawn much attention for their exceptional physical properties such as high melting point, chemical inertness, high incompressibility, and hardness [17]. Similar to nitrogen, nitrogen-rich nitrides with single and double nitrogen bonds have also gained much attention due to their HED applications [18–24]. Recent theoretical calculations have predicted the occurrence of transition metal hexanitrides at high *P-T* such as WN_6, TeN_6, MoN_6, and ReN_6 [12–16]. These hexanitrides are predicted to be stable in a $R\bar{3}m$ structure which contains armchairlike N_6 rings with single bonds between adjacent nitrogen atoms. Tungsten hexanitride (WN_6) stands out in particular because of its high melting point and thermal stability as well as ultrahigh Vickers hardness of ∼57 GPa, the highest among TMNs [13]. WN_6 also possesses unique features of ioniclike crystal and an enlarged band gap under compression [13], which is opposite to normal semiconductors such as silicon. Nitrogen-rich WN_6 has a very good gravimetric and volumetric energy density, making it a potential HED material. Interestingly, WN_6 is predicted to be metastable even at ambient pressure, so it is possible to recover [12,13]. However, the thermodynamic stability pressure for the WN_6 phase predicted by different theoretical models varies significantly from 16 GPa [12] to 65 GPa [13].

This highlights the degree of difficulty to accurately predict the stability and structure of the polynitride phases in correlated transition metals. Most importantly, to the best of our knowledge, the hexazine-bearing TMN has not been synthesized experimentally up to now, so its physical and chemical properties remain unknown experimentally.

High *P-T* conditions are useful to overcome the energy barrier and synthesize new TMN phases. Inspired by a recent theoretical study [13], here we have carried out high *P-T* DAC experiments coupled with *in situ* x-ray diffraction (XRD) measurements up to 165 GPa and 3500 K to explore new chemical compounds in the W-N system. We have successfully synthesized and refined the novel WN_6 phase in the $R\bar{3}m$ structure at 126–165 GPa after heating. Together with high-pressure Raman spectroscopy measurements and theoretical calculations, our results show that the WN_6 phase contains armchairlike hexazine (N_6) rings with strong covalent N—N single bonds stabilized by balanced attractive-repulsive interactions within the crystal structure. These experimental results are used to benchmark new first-principles calculations which further demonstrate ultrahigh hardness and toughness of the WN_6 phase.

Three independent XRD experiments in pulsed laser-heated DACs were carried out on tungsten samples loaded with ultrapure nitrogen at high *P-T* at 13IDD beam line, GSECARS, Advanced Photon Source (see Figs. S2–S4 and a detailed description in Supplemental Material [25]). XRD analysis of the initially loaded tungsten samples showed them to be stable in body-centered cubic (bcc) structure at high pressure without laser heating. After initial laser heating of the W samples surrounded by nitrogen at approximately 114 GPa, new diffraction peaks were observed and can be indexed as $WN_8{\cdot}N_2$ phase which was previously reported [37] (Figs. S3, S4, and S6 in Supplemental Material [25]). In addition, a cg-N phase was observed [7] (Figs. S3 and S4 in Supplemental Material [25]). Upon further heating up to 3500 K at ~126 GPa, many new diffraction peaks appeared (Fig. S3 in Supplemental Material [25]) and they could be indexed to a rhombohedral crystal class with lattice parameters $a = 5.6786(5)$ Å, $c = 4.2057(4)$ Å, and $V = 117.45(5)$ Å^3. With further compression and heating cycles up to the maximum experimental pressure of 165 GPa, diffraction peaks became stronger. All peaks except those corresponding to unreacted W can be well indexed to the rhombohedral phase signaling the stability of the new WN_6 phase at higher pressures [Fig. 1(a)]. Le Bail refinements of the diffraction patterns at 165 GPa confirm that these new peaks correspond to a new phase with the $R\bar{3}m$ structure having lattice parameters of $a = 5.591(1)$ Å and $c = 4.145(1)$ Å [Fig. 1(a)]. The refined space group and lattice parameters are in excellent agreement with the theoretically predicted WN_6 phase with the $R\bar{3}m$ structure

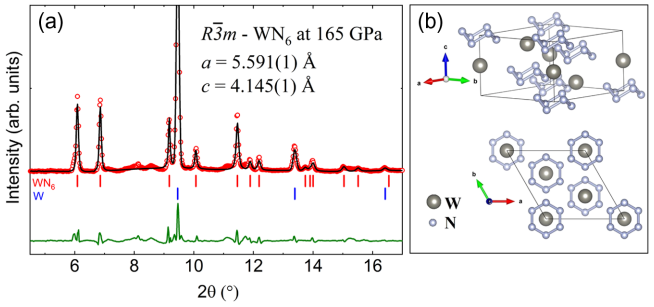

FIG. 1. Crystal structure of the WN_6 phase with the space group $R\bar{3}m$ determined by high-pressure XRD refinement. (a) Le Bail refinement of the WN_6 phase at 165 GPa ($\lambda = 0.3344$ Å) (red vertical ticks). Blue vertical ticks represent unreacted W in the bcc phase that coexists with the WN_6. Red open circles, black line and green line represents the experimental data, the fit and the residual difference respectively. (b) Crystal structure of the WN_6 phase with the novel armchairlike N_6 rings and W atoms in between the rings along the *c* axis [13]. See a representative XRD image at 165 GPa shown in Fig. S5 in Supplemental Material [25].

[12,13] at 165 GPa with lattice parameters $a = 5.596$ Å and $c = 4.144$ Å. In the $R\bar{3}m$-structured WN_6 phase, nitrogen atoms form novel armchairlike N_6 rings and tungsten atoms sit midway in between two N_6 rings along the crystallographic *c* axis [Fig. 1(b)] [13]. Further, during the decompression cycles, the diffraction peaks for the WN_6 phase could be found to pressures as low as 68 GPa, before the unfortunate breaking of one of the diamonds. cg-N and $WN_8{\cdot}N_2$ phases also coexisted with WN_6 up to 152 GPa in compression and up to 68 GPa in the decompression cycle (Fig. S3 in Supplemental Material [25]). In the brief recount, our experimental results show the occurrence of the $R\bar{3}m$-structured WN_6 phase at pressures between 126 and 165 GPa after laser heating (Fig. S7 in Supplemental Material [25]).

High-pressure micro-Raman measurements [38] of the laser-heated areas for the WN_6 phase and theoretical predictions of the vibrational modes at the Γ point were performed to better understand the nature of the N_6 rings and vibrational symmetries in the WN_6 phase. Raman spectra of the WN_6 phase recorded at 165 GPa display intense peaks at around 760, 905, and 1057 cm^{-1} [Fig. 2(a)]. Factor group analysis for possible vibrational modes in $R\bar{3}m$-structured WN_6 phase shows that 21 zone center vibrational phonon modes can be assigned as $\Gamma = 2A_{1g} + A_{1u} + A_{2g} + 3A_{2u} + 3E_g + 4E_u$. Out of these, a total of five different $(2A_{1g} + 3E_g)$ Raman-active modes are expected in 400–1600 cm^{-1} wave number range [Fig. 2(a)]. These theoretically calculated modes [red vertical ticks in Fig. 2(a)] are generally in good agreement with the experimental peak positions. Direct comparison between theory and experiments indicates that the vibrational mode around 1057 cm^{-1} arises from A_{1g} symmetry,

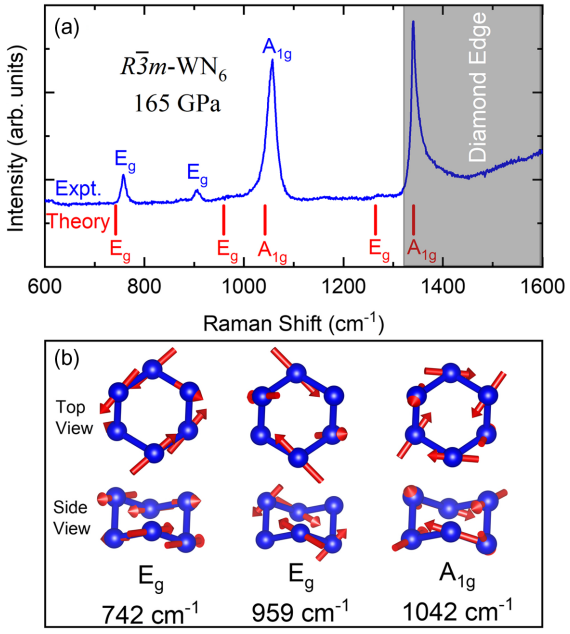

FIG. 2. Representative Raman spectrum and eigenvectors of the $R\bar{3}m$-structured WN_6 phase at high pressure. (a) Raman spectrum of the WN_6 phase recorded at 165 GPa (excitation wavelength, $\lambda = 532$ nm). The red vertical ticks represent positions of theoretical Raman-active modes of the WN_6 phase. Based on the comparison with theory, experimentally observed peaks are assigned vibrational symmetries labeled next to the peaks. (b) Eigenvectors for three experimentally observed modes. Symmetries and theoretically calculated equivalent Raman shifts are also labeled for clarity. The red arrows indicate the direction and magnitude of nitrogen atomic displacements in the N_6 rings, as viewed from the top and the side.

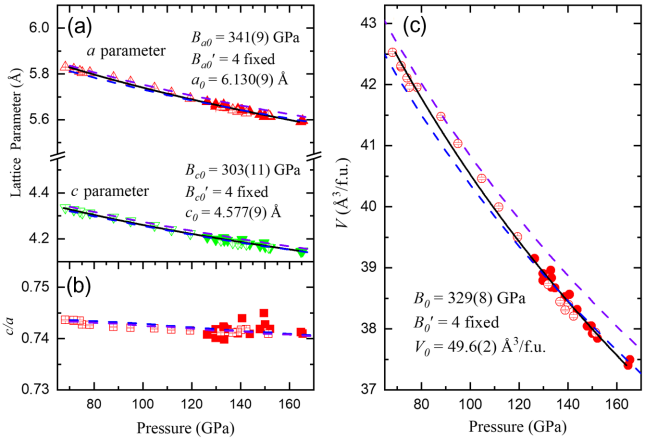

FIG. 3. Unit cell parameters and volume of the $R\bar{3}m$-structured WN_6 phase at high pressure. (a) Pressure-dependent unit cell parameters of the WN_6 phase from XRD results. Solid and open red triangles represent a parameter in compression and decompression cycle, respectively. Solid and open green triangles represent c parameter in compression and decompression cycle, respectively. Black continuous lines represent fitting of the axial incompressibility using third-order B-M EOS. Violet and blue dashed lines represent the calculated EOS by PBE and PBE-D3 functional. (b) Pressure dependence of experimental c/a ratio compared with calculated c/a. Red solid and open squares are experimental data for compression and decompression cycle, respectively. Violet and blue dashed lines represent data calculated by PBE and PBE-D3 functional, respectively. (c) Pressure-dependent unit cell volume of WN_6 fitted by third-order B-M EOS. Solid and open red circles represent volume in compression and decompression cycle, respectively, and the black line represents fitted EOS. Experimental EOS was compared with the theoretical results using plain PBE (violet dashed line) and PBE-D3 (blue dashed line) functionals.

while both 760 and 905 cm^{-1} vibrations are assigned to be of E_g symmetry. The agreement here leads us to use the eigenvectors for the experimentally observed Raman modes to illustrate the magnitude and direction of the nitrogen atomic displacements in the N_6 rings [red arrows in Fig. 2(b)]. All three eigenvectors represent coupled motions for the opposite nitrogen atoms in the N_6 rings, which are characteristic of the armchairlike single-bonded N_6 vibrations. In particular, the symmetric stretching motions of opposite nitrogen atoms viewing from the top view of the N_6 ring contribute to the characteristic Raman peaks at 1057 cm^{-1} of the A_{1g} symmetry. Our experimental observation and theoretical predictions of the high-wave-number A_{1g} vibration mode at 1057 cm^{-1} confirm the single-bonding character between adjacent nitrogen atoms in the N_6 rings of the WN_6 phase (Figs. 1 and 2). The observation of this high-wave-number Raman peak is consistent with experimentally observed Raman shift range in other single-bonded polymeric nitrogen phases such as cg-N and bp-N: all these phases display vibrational modes around the 800–1300 cm^{-1} range at megabar pressure region corresponding to single-bonded nitrogen vibrations (Fig. S8 in Supplemental Material [25]) [3–5,7].

Pressure-dependent unit cell parameters, d spacings, and unit cell volumes of the WN_6 phase are obtained from refinements of the XRD spectra in the pressure range of 68–165 GPa (Fig. 3 herein and Fig. S9 of Supplemental Material [25]). Using third-order Birch-Murnaghan (B-M) equation of state (EOS) to fit the experimental data, axial incompressibility of the WN_6 phase are 341(9) GPa for the a axis and 303(11) GPa for the c axis. These means that the c/a ratio is nearly constant with pressure within uncertainties [Fig. 3(a) and 3(b)]. The EOS parameters for WN_6 are $B_0 = 329(8)$ GPa with $B_0' = 4$ fixed and $V_0 = 49.6(2)$ Å^3/f.u. B_0 is found to be in good agreement with a theoretically predicted value of 302.7 GPa [13], supporting the highly incompressible nature of the WN_6 phase. New theoretical calculations performed to estimate lattice and EOS parameters by Perdew-Burke-Ernzerhof (PBE) and PBE-D3 functionals, and the results are consistent with these experimental parameters [Figs. 3(a) and 3(b)]. The high-pressure EOS curve calculated by the PBE functional [violet dashed line in Fig. 3(c)] agrees with the experimental results at pressures below 90 GPa. With further

compression, the PBE results exhibit an increasing difference of larger volume compared to the experimental values. This may originate from ignoring weak noncovalent interactions between the quasimolecular N_6 rings, which could shrink the unit cell at high pressures. Based on a previous report, each covalent-bonded N_6 ring obtains around $2.4e$ Bader charge [13]. Similar order of the charge transfer is also found in the N_6 rings of TeN_6 [15]. These motivate us to investigate the weak noncovalent interactions between N_6 rings. The weak noncovalent interactions were taken into account by employing the DFT-D3 dispersion correction method in the revised PBE-D3 functional [39,40]. The calculated lattice parameters and volume after this correction are found to be in better agreement with the experimental data especially in the pressure range of 120–170 GPa, as shown by the blue dashed lines in Fig. 3. These results highlight that the rhombohedral unit cell of WN_6 is extremely stiff yet experiences almost isotropic compression that reflects balanced contributions of the strong covalent nitrogen rings, the attractive ionic interactions between W and N_6 rings, and the repulsive interactions between the N_6 rings [Figs. 1(b) and 3(b)].

Further, the EOS parameters of the WN_6 phase are compared with other single-bonded polymeric nitrogen phases (Table S1 in Supplemental Material [25]) to understand the behavior of single-bonded nitrogen sublattices at high pressure. The incompressibility of the WN_6 is relatively higher than those in cg-N [$B_0 = 298(6)$ GPa] [7] and bp-N ($B_0 = 183$ GPa) [4], but is comparable with that in HLP-N [$B_0 = 349(40)$ GPa] [1]. This observation indicates that the N_6 structural unit in WN_6 is very stiff and plays an essential role in the ultrahigh incompressibility of the WN_6 unit cell. To better understand the effect of the weak noncovalent interactions between the N_6 rings on the lattice and EOS parameters, further calculations were performed using charge-density-based methods. Weak noncovalent interactions are observed directly by calculating two- and three-dimensional reduced density gradient (Fig. S10 in Supplemental Material [25]). The noncovalent interactions such as the attractive interactions between W atoms and N_6 rings and repulsive interactions between the N_6 rings coexist in WN_6. The coexistence of these interactions compensates for each other to stabilize the armchairlike hexazine rings in WN_6 at high pressures and contributes to its ultrahigh incompressibility. Furthermore, the calculated nearest N—N bond length in the WN_6 phase is 1.46 Å at ambient pressure and 1.39 Å at 130 GPa. Among the known polymeric nitrogen phases, HLP-N also consists of distorted N_6 ring structure; however, this phase is only found to be stable above 240 GPa. The nearest N—N bond length of HLP-N is 1.30 Å at 235 GPa [1], whereas it is 1.31 Å at 400 GPa in the WN_6 phase. In comparison, the nearest bond length for single-bonded nitrogen atoms is 1.346(4) Å in cg-N at 115 GPa [7] and is 1.338(6) Å in bp-N at 140 GPa [3]. Notably, N—N bond length in the range ~1.30–1.46 Å corresponds to high incompressibility. Interestingly, the WN_6 phase is found to have the longest N—N bond length between nearest nitrogen atoms (N-N) among different TMNs [Fig. 4(a)]. That means, other nitrogen-rich nitrides with single-bonded nitrogen and long nearest N—N bond lengths could also be highly incompressible.

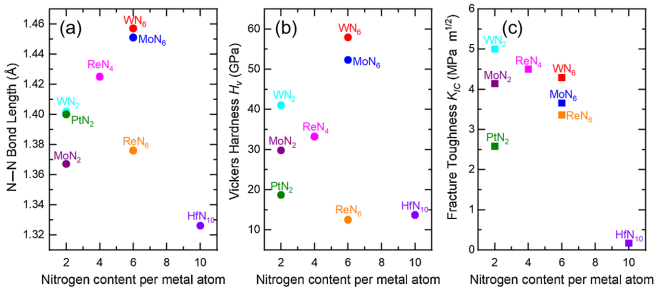

FIG. 4. Comparisons of the bond length, hardness, and toughness of the WN_6 phase with other relevant nitrides. (a) Theoretically calculated nearest N—N bond length for representative nitrides with nitrogen content (x) per metal atom (WN_6 [13], MoN_6 [14], ReN_6 [14], $P4/mbm$ WN_2 [41] and MoN_2 [42], $Cmmm$ ReN_4 [43], $Immm$ HfN_{10} [44], and pyrite-type PtN_2 [45]). (b) The theoretically calculated Vickers hardness (H_v, GPa) for different nitrides with nitrogen content (x) per metal atom. The hardest known transition metal (M) nitrides (MN_x) are compared. (c) The calculated fracture toughness (K_{IC}, MPa m$^{1/2}$) for different nitrides with nitrogen content (x) per metal atom. Several MN_x with high toughness are selected for comparison.

In order to better understand the mechanical properties of the WN_6 phase, full elastic constants (C_{ij}'s) of the WN_6 phase are also calculated at ambient pressure (Table S2 in Supplemental Material [25]). The bulk modulus (B) and shear modulus (G) of the WN_6 phase at ambient pressure are calculated from the C_{ij}'s and its density, which are 302.7 and 315.7 GPa, respectively (Table S3 in Supplemental Material [25]). For a detailed comparison, the C_{ij} and mechanical moduli (B and G) from previously reported nitrides with different nitrogen content are listed in Tables S2 and S3, respectively, see Supplemental Material [25], including the isostructural MoN_6 and ReN_6 [14], $P4/mbm$ WN_2 [41] and MoN_2 [42], $Cmmm$ ReN_4 [43], $Immm$ HfN_{10} [44], and pyrite-type PtN_2 [45]. As shown in Table S3 in Supplemental Material [25], the $R\bar{3}m$-structured WN_6 phase has the highest G among the known transition metal nitrides. Based on the widely used semiempirical models by Chen *et al.* [46] and Tian *et al.* [47], we estimated the Vickers hardness H_v of all the relevant transition metal nitrides. The WN_6 phase is found to be superhard and possesses the highest Vickers hardness (57.9 GPa) among the nitrides [Fig. 4(b)]. The nearest N—N bond length is showing a nearly consistent relation with the hardness of TMNs [Figs. 4(a) and 4(b)]. The fracture toughness (K_{IC}) for different nitrides was calculated using the empirical model

by Niu *et al.* [48] [Fig. 4(c) herein and Table S3 in Supplemental Material [25]]. With G of 315.7 GPa and a low Pugh modulus ratio B/G of 0.96, the WN_6 phase can reach a high K_{IC} of around 4.29 MPa $m^{1/2}$. This value is slightly below those of WN_2 and ReN_4 but can be considered high because materials with high hardness usually tend to have low K_{IC} values. Our calculations here indicate that WN_6 has a good balance between superhardness and fracture toughness, which is important for material science applications. Based on theoretical calculations [13], the superhardness of the WN_6 phase can be attributed to the electron repulsion between W and N atoms that helps to open the electronic band gap and results in the nonmetallicity in WN_6.

In summary, we have successfully synthesized the $R\bar{3}m$-structured WN_6 phase at 126–165 GPa after laser heating up to ~3500 K. The WN_6 phase contains novel armchairlike N_6 rings that are manifested in the E_g and A_{1g} Raman-active modes at 760, 905, and 1057 cm^{-1}. The refined lattice parameters and Raman-active modes of the WN_6 phase are in excellent agreement with theoretical calculations. The strong covalent N—N single bonds in the N_6 ring, the ionic interactions between the N_6 rings and the tungsten atoms, and the repulsive electrostatic interactions between N_6 rings are the main attributes of the ultrahigh incompressibility of the WN_6 phase. The armchairlike hexazine nitrogen sublattice in the WN_6 phase is remarkably comparable to that in the polymeric nitrogen phases and can be a high-energy-density material candidate. Calculations of the elastic moduli indicate that the WN_6 phase exhibits superhardness and good fracture toughness. Future efforts in the synthesis and recovery of TMNs will lead to a wealth of knowledge in the novel chemistry and physical properties of the single-bonded hexazine-bearing nitrides.

N. P. S. acknowledges the postdoctoral fellowship support at the Center for High Pressure Science and Technology Advanced Research (HPSTAR). N. P. S. and J. L. acknowledges the financial support by the National Natural Science Foundation of China (Grant No. U1930401). J. S. gratefully acknowledges financial support from the National Key R&D Program of China (Grant No. 2016YFA0300404), the National Natural Science Foundation of China (Grants No. 11974162 and No. 11834006), the Fundamental Research Funds for the Central Universities. K. X. acknowledges the financial support from the National Natural Science Foundation of China (Grant No. 12004185) and the project funded by China Postdoctoral Science Foundation (Grant No. 2019M651767). Y. Z. acknowledges support from the National Natural Science Foundation of China (Grants No. 11872077 and No. 41804082). The numerical calculations in this Letter were performed on the computing facilities in the High Performance Computing Center of Collaborative Innovation Center of Advanced Microstructures, the High Performance Computing Center (HPCC) of Nanjing University, the High Performance Computing Center Facility of Nanjing Forestry University, and "Tianhe-2" at NSCC-Guangzhou. XRD experiments were conducted at GeoSoilEnviroCARS of Advanced Photon Source (APS), Argonne National Laboratory (ANL). GeoSoilEnviroCARS operations are supported by the National Science Foundation-Earth Sciences (No. EAR-1634415) and the Department of Energy, Geosciences (No. DE-FG02-94ER14466). Part of this research used resources of the Advanced Photon Source, a U.S. Department of Energy (DOE) Office of Science User Facility operated for the DOE Office of Science by Argonne National Laboratory under Contract No. DE AC02-06CH11357.

*Corresponding author.
nilesh@uic.edu
†Corresponding author.
jin.liu@hpstar.ac.cn
‡Corresponding author.
jiansun@nju.edu.cn
§Corresponding author.
afu@jsg.utexas.edu
¶Present address: Department of Physics, University of Illinois at Chicago, Chicago, Illinois 60607, USA.

[1] D. Laniel, G. Geneste, G. Weck, M. Mezouar, and P. Loubeyre, Phys. Rev. Lett. **122**, 066001 (2019).
[2] M. J. Greschner, M. Zhang, A. Majumdar, H. Liu, F. Peng, J. S. Tse, and Y. Yao, J. Phys. Chem. A **120**, 2920 (2016).
[3] D. Laniel, B. Winkler, T. Fedotenko, A. Pakhomova, S. Chariton, V. Milman, V. Prakapenka, L. Dubrovinsky, and N. Dubrovinskaia, Phys. Rev. Lett. **124**, 216001 (2020).
[4] C. Ji, A. A. Adeleke, L. Yang, B. Wan, H. Gou, Y. Yao, B. Li, Y. Meng, J. S. Smith, V. B. Prakapenka, W. Liu, G. Shen, W. L. Mao, and H. K. Mao, Sci. Adv. **6**, eaba9206 (2020).
[5] D. Tomasino, M. Kim, J. Smith, and C.-S. Yoo, Phys. Rev. Lett. **113**, 205502 (2014).
[6] M. J. Lipp, J. P. Klepeis, B. J. Baer, H. Cynn, W. J. Evans, V. Iota, and C. S. Yoo, Phys. Rev. B **76**, 014113 (2007).
[7] M. I. Eremets, A. G. Gavriliuk, I. A. Trojan, D. A. Dzivenko, and R. Boehler, Nat. Mater. **3**, 558 (2004).
[8] C. J. Pickard and R. J. Needs, Phys. Rev. Lett. **102**, 125702 (2009).
[9] A. K. McMahan and R. LeSar, Phys. Rev. Lett. **54**, 1929 (1985).
[10] T.-K. Ha, R. Cimiraglia, and M. T. Nguyen, Chem. Phys. Lett. **83**, 317 (1981).
[11] H. Huber, Angew. Chem., Int. Ed. Engl. **21**, 64 (1982).
[12] Q. Li, L. Sha, C. Zhu, and Y. Yao, Europhys. Lett. **118**, 46001 (2017).
[13] K. Xia, H. Gao, C. Liu, J. Yuan, J. Sun, H.-T. Wang, and D. Xing, Sci. Bull. **63**, 817 (2018).
[14] Q. Wei, C. Zhao, M. Zhang, H. Yan, and B. Wei, Phys. Lett. A **383**, 2429 (2019).

[15] Z. Liu, D. Li, Q. Zhuang, F. Tian, D. Duan, F. Li, and T. Cui, Commun. Chem. **3**, 42 (2020).
[16] C. Lu and C. Chen, Phys. Rev. Mater. **4**, 043402 (2020).
[17] V. L. Solozhenko and E. Gregoryanz, Mater. Today **8**, 44 (2005).
[18] C. Zhang, C. Sun, B. Hu, C. Yu, and M. Lu, Science **355**, 374 (2017).
[19] B. A. Steele, E. Stavrou, J. C. Crowhurst, J. M. Zaug, V. B. Prakapenka, and I. I. Oleynik, Chem. Mater. **29**, 735 (2017).
[20] S. Wei, D. Li, Z. Liu, X. Li, F. Tian, D. Duan, B. Liu, and T. Cui, Phys. Chem. Chem. Phys. **19**, 9246 (2017).
[21] D. Laniel, G. Weck, G. Gaiffe, G. Garbarino, and P. Loubeyre, J. Phys. Chem. Lett. **9**, 1600 (2018).
[22] Z. Liu, D. Li, S. Wei, Y. Liu, F. Tian, D. Duan, and T. Cui, Phys. Lett. A **383**, 125859 (2019).
[23] Z. Liu, D. Li, Y. Liu, T. Cui, F. Tian, and D. Duan, Phys. Chem. Chem. Phys. **21**, 12029 (2019).
[24] K. Xia, X. Zheng, J. Yuan, C. Liu, H. Gao, Q. Wu, and J. Sun, J. Phys. Chem. C **123**, 10205 (2019).
[25] See Supplemental Material at http://link.aps.org/supplemental/10.1103/PhysRevLett.126.065702 for experimental and theoretical calculations details, Tables S1–S3, Figs. S1–S10, and bibliography, which includes Refs. [26–36].
[26] W. Humphrey, A. Dalke, and K. Schulten, J. Mol. Graphics **14**, 33 (1996).
[27] G. Kresse and J. Furthmüller, Phys. Rev. B **54**, 11169 (1996).
[28] J. P. Perdew, K. Burke, and M. Ernzerhof, Phys. Rev. Lett. **77**, 3865 (1996).
[29] G. Shen, M. L. Rivers, Y. Wang, and S. R. Sutton, Rev. Sci. Instrum. **72**, 1273 (2001).
[30] V. B. Prakapenka, A. Kubo, A. Kuznetsov, A. Laskin, O. Shkurikhin, P. Dera, M. L. Rivers, and S. R. Sutton, High Press. Res. **28**, 225 (2008).
[31] A. Otero-de-la-Roza, M. A. Blanco, A. M. Pendás, and V. Luaña, Comput. Phys. Commun. **180**, 157 (2009).
[32] E. R. Johnson, S. Keinan, P. Mori-Sánchez, J. Contreras-García, A. J. Cohen, and W. Yang, J. Am. Chem. Soc. **132**, 6498 (2010).
[33] K. Momma and F. Izumi, J. Appl. Crystallogr. **44**, 1272 (2011).
[34] A. Otero-de-la-Roza, E. R. Johnson, and V. Luaña, Comput. Phys. Commun. **185**, 1007 (2014).
[35] C. Prescher and V. B. Prakapenka, High Press. Res. **35**, 223 (2015).
[36] A. Togo and I. Tanaka, Scr. Mater. **108**, 1 (2015).
[37] M. Bykov, S. Chariton, E. Bykova, S. Khandarkhaeva, T. Fedotenko, A. V. Ponomareva, J. Tidholm, F. Tasnadi, I. A. Abrikosov, P. Sedmak, V. Prakapenka, M. Hanfland, H. P. Liermann, M. Mahmood, A. F. Goncharov, N. Dubrovinskaia, and L. Dubrovinsky, Angew. Chem., Int. Ed. Engl. **59**, 10321 (2020).
[38] N. Holtgrewe, E. Greenberg, C. Prescher, V. B. Prakapenka, and A. F. Goncharov, High Press. Res. **39**, 457 (2019).
[39] S. Grimme, S. Ehrlich, and L. Goerigk, J. Comput. Chem. **32**, 1456 (2011).
[40] S. Grimme, J. Antony, S. Ehrlich, and H. Krieg, J. Chem. Phys. **132**, 154104 (2010).
[41] H. Yan, M. Zhang, Q. Wei, and P. Guo, J. Alloys Compd. **581**, 508 (2013).
[42] S. Yu, B. Huang, X. Jia, Q. Zeng, A. R. Oganov, L. Zhang, and G. Frapper, J. Phys. Chem. C **120**, 11060 (2016).
[43] Z. Zhao, K. Bao, D. Li, D. Duan, F. Tian, X. Jin, C. Chen, X. Huang, B. Liu, and T. Cui, Sci. Rep. **4**, 4797 (2014).
[44] J. Zhang, A. R. Oganov, X. Li, and H. Niu, Phys. Rev. B **95**, 020103(R) (2017).
[45] J. C. Crowhurst, A. F. Goncharov, B. Sadigh, C. L. Evans, P. G. Morrall, J. L. Ferreira, and A. J. Nelson, Science **311**, 1275 (2006).
[46] X.-Q. Chen, H. Niu, D. Li, and Y. Li, Intermetallics **19**, 1275 (2011).
[47] Y. Tian, B. Xu, and Z. Zhao, Int. J. Refract. Met. Hard Mater. **33**, 93 (2012).
[48] H. Niu, S. Niu, and A. R. Oganov, J. Appl. Phys. **125**, 065105 (2019).